

Measurements of dose distributions in alanine using EPR imaging

Mathias Anton, Hans-Joachim Selbach

Physikalisch-Technische Bundesanstalt,
Bundesallee 100, 38116 Braunschweig

Introduction

Ionising radiation produces stable free radicals in alanine, an amino acid. The radicals can be detected via electron paramagnetic resonance (EPR). The radiation transport properties of alanine are very close to those of water, which makes it useful for dosimetry in radiation therapy. A measure for the effect caused by ionising radiation in human tissue is the absorbed dose to water D_w . The *International Commission on Radiation Units and Measurement* requires in its report 24 [1], that the uncertainty of the dose applied to the target volume of the patient should be $\leq 5\%$ at a confidence level of 95 %.

Several national metrology institutions employ the alanine/EPR dosimetry system as a secondary standard for the measurement of D_w , such as the NPL (UK, [2]), the NIST (USA, [3]), the ISS (Italy, [4]) and the Physikalisch-Technische Bundesanstalt PTB (GER, [5]). The relative standard measurement uncertainty for $D_w \geq 10$ Gy using alanine/EPR is 1% or less.

The goal of the present investigation is the assessment of the possibilities of alanine EPR imaging (EPRI) for the determination of one-, two- or three-dimensional dose distributions. Precise determination of dose distributions in a relatively small volume may be useful for the characterisation of radiation fields in the vicinity of brachytherapy sources as well as for special cases in teletherapy when extremely steep gradients of the dose distributions are required, e.g. if an organ at risk is close to the target volume. This is especially important for modern forms of 3D conformal radiotherapy such as the so-called intensity modulated radiotherapy (IMRT, see e.g. [6, 7, 8]).

Although depth dose curves have already been studied using EPR imaging [9, 10], significant progress has been made in recent years concerning the availability of powerful measuring instruments such as Bruker's ELEXSYS spectrometer, which made revisiting the subject worthwhile. In order to quantify the resolution achievable with the ELEXSYS spectrometer and alanine detectors, two alanine/paraffin probes with strongly varying dose distributions were tested.

Irradiation of probes

Cylindrical probes with a diameter of 4.8 mm and a height of 10 mm, which consist of alanine and paraffin as a binder were purchased from Wieser Messtechnik (München). They were irradiated using the PTB's β -particle planar source reference field ($^{90}\text{Sr}/^{90}\text{Y}$, $\varnothing = 15$ mm). The probes were centered within a cylindrical PMMA phantom with a diameter of 25 mm and a height of 15 mm. The thickness of the PMMA layer between the source's surface and the nearest surface of the probe was 2 mm. One of the probes (E2) was irradiated

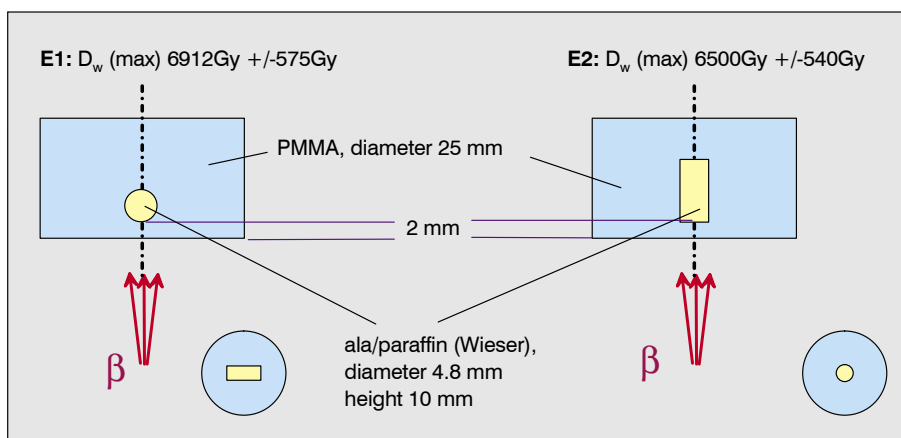


Fig. 1: Irradiation geometry for probes E1 (left) and E2 (right)

with its axis parallel to the surface normal of the source, another one (E1) was irradiated with its axis perpendicular to the surface normal (Fig. 1), both with a dose of ≈ 6 kGy at the maximum. Due to the limited range of the β -particles the dose drops fast with increasing depth (Fig. 4).

Radiation transport simulations

For the E2 probe (symmetry axis parallel to the symmetry axis of the reference field), the spatial distribution of the absorbed dose was calculated using the MCNP Monte Carlo radiation transport software.

Results of MCNP calculations had been verified before using 2D profiles measured with ionisation chambers and can thus be considered as a reference for the shape of the dose distribution of the β radiation field. The average dose absorbed in cylindrical alanine/paraffin discs of 0.5 mm height was calculated, yielding the depth dose curve. The depth-dose curve was then "re-distributed" to a three-dimensional voxel model taking the known spatial distribution of the reference field into account.

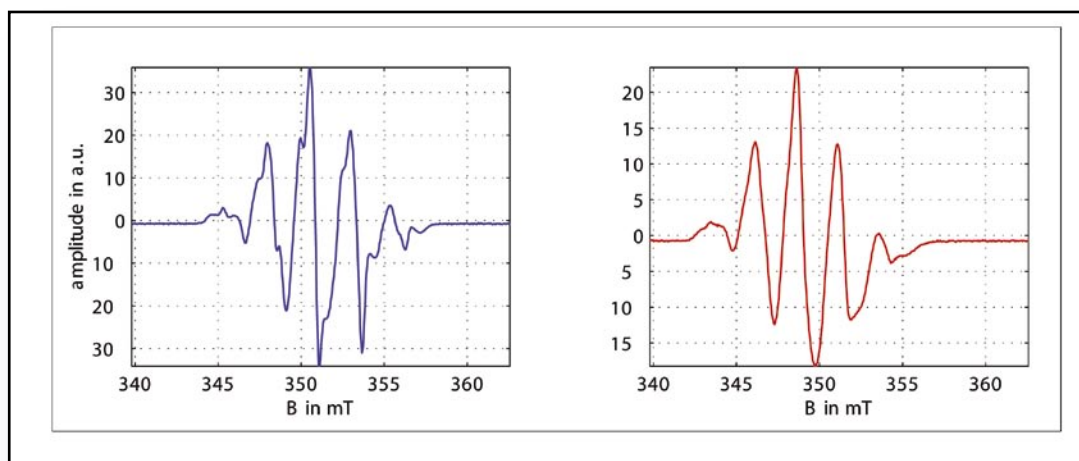


Fig. 2: left: alanine spectrum, zero gradient; right: measured 1D profile of probe E2 with a gradient of 0.48 mT/mm along the axis.

EPR Measurements

Spatial resolution in EPR measurements is achieved by applying additional gradients of the flux density B [10]. A Bruker ELEXSYS X-Band EPR imaging system with three-axis planar gradients was used. 1D, 2D and 3D images were reconstructed from projections measured with a B -gradient of 0.48 mT/mm and a field sweep of 22.79mT. For the 1D case, one projection was sufficient while for 2 and 3 dimensions 78 and 2209 projections were used, respectively. **Fig. 2** shows the alanine spectrum measured without any gradient of the B -field together with the profile obtained with a gradient of 0.48 mT/mm along the axis of probe E2. The signal-to-noise ratio S/N of the measured profile was ≈ 700 . Broadening and distortion of the measured profile (Fig.2) due to the complex line shape of the alanine spectrum were removed by deconvolution, using the zero gradient alanine spectrum as the instrument function (the deconvolution result is denoted as "projection"). For 2D and 3D images, filtered back projection was applied to reconstruct the spatial distribution from the measured projections.

EPR measurements as well as the reconstructions were carried out by Bruker using the ELEXSYS' Xepr software. In addition, a maximum entropy algorithm (MaxEnt), a first order regularisation method and a regularisation method making use of the Fisher-information (MinFisher) were compared to a Fourier method which is part of the Xepr software. The three first methods had been applied to soft-Xray tomography before and are described in detail in [11], additional information can be found e.g. in [12, 13]. The algorithms were implemented in MATLAB (The MathWorks Inc.).

Results

Fig. 3 compares the deconvolution results that have been obtained using the four different algorithms. The result of the Fourier method exhibits a severe drawback of the method that was mentioned in [13]: noise tends to be amplified by the deconvolution process. The artefacts displayed can only be avoided in case of noise-"free" signals. The first order regularisation method produces slightly smaller artefacts. This advantage is compensated by a broadening of the reconstructed feature which is inherent to the method, since the regularising function in this case is the norm of the gradient of the curve to be reconstructed. The method denoted as MinFisher yields a narrower curve with significantly smaller artefacts than the first order regularisation. The advantage of the MinFisher approach was already demonstrated in [11]: the regularising function is the norm of the gradient (as in the case of first order regularisation), but this time weighted with the inverse value of the reconstructed function itself. This means, the effective "smoothing" induced by the regularising function is stronger in regions with a small signal while regions with large signals are not smoothed. The MaxEnt result finally appears to exhibit the smallest artefacts. One of the reasons for this may be a

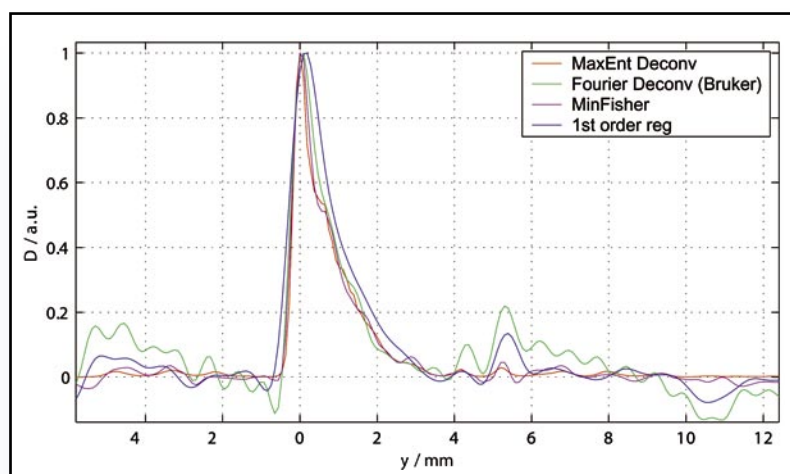


Fig. 3: Reconstructed depth dose curve, probe E2. red: 1D measurement, MaxEnt deconvolution; green: Fourier (Xepr); magenta: Minimum Fisher Information; blue: first order regularisation.

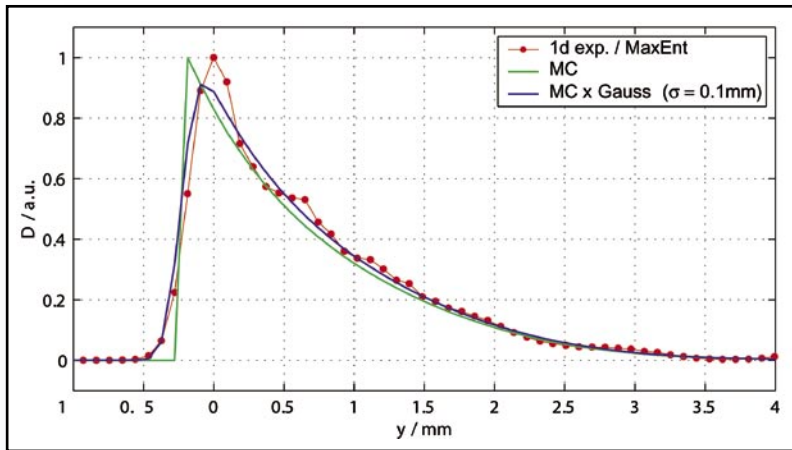
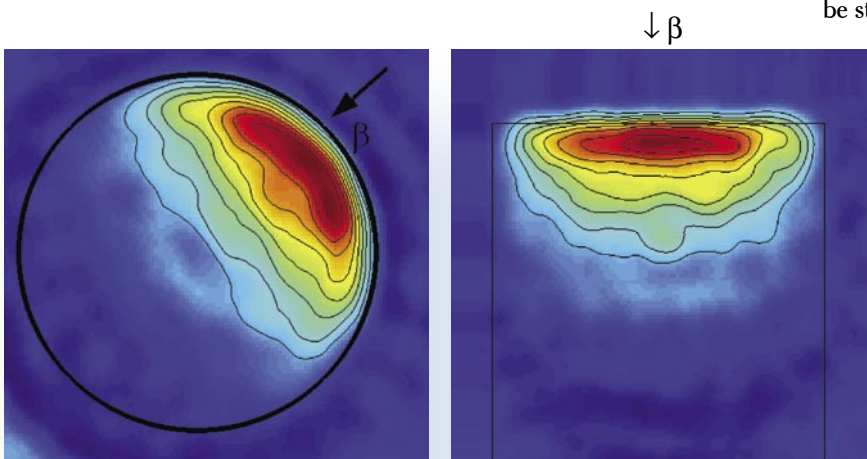


Fig. 4: Reconstructed depth dose curve, probe E2. Red: 1D measurement, MaxEnt deconvolution; green: MC calculation; blue: MC calculation convolved with a Gaussian ($\sigma=0.1\text{mm}$). The y-axis of the deconvolution result was shifted to achieve optimum agreement between calculation and measurement.

feature common to all MaxEnt algorithms: the function to be recovered is assumed to be a probability distribution function, therefore no negative values can occur. In the region with a large signal amplitude the results of MaxEnt and MinFisher are very close to each other and to the Fourier result.

Fig. 4, the MaxEnt reconstruction is compared to the MC-simulated depth dose curve. The theoretical curve is displayed "as is" and, in addition, convolved with a Gaussian in order to model the finite resolution. The half width σ of the Gaussian was in this case 0.1 mm. All curves were normalised using a least-squares fit to facilitate the comparison. The amplitude of some artefacts as well as deviations from the theoretical curve reach 10 – 20 % of the maximum amplitude, which is considered too large in view of the requirements of therapy dosimetry. In order to quantify the dependence of the resolution on the signal-to-noise ratio S/N, artificial noise (Gaussian, by a random number generator) was added to the measured profile.



The deconvolution results showed that for $S/N=200 \dots 20$, the resolution dropped from 0.15 mm to 0.3 mm. For $S/N < 20$, no reasonable results were achieved. In case of lower dose values, the S/N required to obtain optimum resolution can be produced by using longer acquisition times t , where $S/N \propto \sqrt{t}$. This is no severe restriction as long as only one-dimensional distributions are sought.

Examples for 2D reconstructions are displayed in **Fig. 5**. The left part shows a 2D image of probe E1 whereas the right part displays a 2D image of probe E2. The shape of the probe is indicated by the black circle and the black rectangle, respectively. The dark blue areas of the image correspond to negative values of the reconstructed distributions. This fact as well as the distortions of the isodose contours are probably due to artefacts of the deconvolution procedure which are propagated by the tomographic reconstruction. The rounded contours on the right part (E2) are a purely geometrical effect, since the 2D reconstructions corresponds to a projection of the cylindrical volume to a plane.

Fig. 6 shows a cross section and two different slices of the 3D dose distribution of probe E2. Part a) of Figure 6 shows a cross section of the simulated 3D dose distribution for probe E2. The slight asymmetry (which is also obvious from the radial profile, see e)) is due to the fact that the symmetry axis of the β -radiation field does not exactly coincide with the symmetry axis of the irradiated detector. The theoretical profile was convolved with a Gaussian in order to model the experimental resolution limit, which is shown in part b) of **Fig. 6**. This should be compared to the cross section of the experimental 3D reconstruction which is displayed in part c) of the same figure. The radial distribution of the dose (in arbitrary units) and the distribution along the axis of the cylindrical E2 probe are displayed in part d) and e) of **Fig. 6**, respectively. The green curves of d) and e) correspond to the simulated distribution shown in a), the blue ones represent the convolved and hence broadened distribution shown in b) while the red curves finally show the experimental results. While good agreement of the depth dose curves e) can be stated, the measured radial profile appears somewhat too narrow. This is possibly due to the fact that the radial dependence of the sensitivity of the resonator was not taken into account. As in the 2D case (Figure 5), some distortions of the profiles and isodose contours are observed which are probably due to artefacts from the deconvolution process.

Fig. 5: Left: 2D image of probe E1, irradiated from one side (see arrow); **Right:** 2D image of probe E2, irradiated from the top.

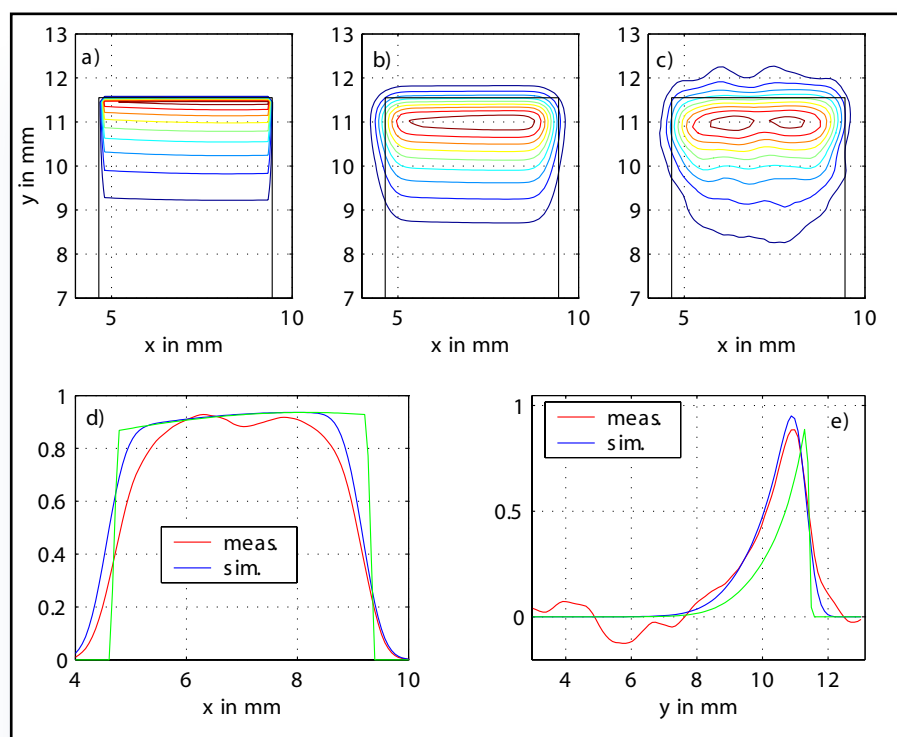


Fig. 6: 3D distribution for probe E2. a): cross section of the MC simulation; b): cross section of the simulation convolved with a Gaussian; c): cross section of the measured distribution; d): radial profile, e): profile along the axis. For d) and e) the green curve corresponds to a), the blue one to b) and the red one represents the experimental result c).

One-dimensional slices (depth-dose curves) through both the 2D and the 3D images of probe E2 were compared to the MC depth dose curve. From a comparison between the image reconstruction and the theoretical curve convolved with a Gaussian (as described above), the resolution deduced from the 3D image was 0.3mm and for the 2D image, 0.2mm was achieved. For the 1D measurement, 0.1mm was obtained (see Fig. 4).

Conclusions

In summary, EPRI with alanine allows the determination of dose distributions in one, two and three dimensions on a scale of a few tenths of a mm. Determination of depth dose curves is possible with a resolution of 0.1mm if a signal-to-noise ratio of ≈ 500 can be achieved. However, the deviations between measured and calculated depth dose curves of up to 10% indicate that the uncertainties achievable with EPRI and alanine will probably be too large for applications in radiotherapy.

Unfortunately, the immense capabilities of the ELEXSYS imaging system can not be exploited using the alanine detector. Reasons for this are the huge linewidth (0.5mT for the central line) together with the complex spectrum of alanine as well as the comparatively low concentration of spins induced per unit absorbed radiation energy, which apparently impose limits on the quality of the reconstruction. If a

substance could be identified which combined a high radiation yield with a small line width, EPRI would be a wonderful instrument for measuring multidimensional dose distributions on a very small scale.

The quality of the reconstructions for probes with a comparatively low concentration of spins can probably be improved if a deconvolution algorithm that is more stable with respect to noisy data is integrated to the Xepri software. For 2D and 3D distributions, incorporation of the radial variation of the sensitivity of the resonator may be useful as well, if very precise results are required.

Acknowledgements

The authors wish to thank Dr. P. Höfer, Dr. A. Kamlowski and B. Gehrhoff (Bruker Biospin, Karlsruhe) for making this investigation possible, for producing the experimental EPRI data, and for many helpful discussions. Thanks are also due to Dr. M. Bambynek (PTB) for irradiating the probes.

References

- [1] ICRU. *ICRU Report 24*, Determination of Absorbed Dose in a Patient Irradiated by Beams of X or Gamma Rays in Radiotherapy Procedures. International Commission on Radiation Units and Measurements, Washington D.C., USA, 1976.
- [2] P H G Sharpe, K Rajendran, and J P Sephton. Progress towards an Alanine/ESR therapy level reference dosimetry service at NPL. *Applied Radiation and Isotopes*, 47(11/12):1171-1175, 1996.
- [3] V Nagy. Accuracy considerations in EPR dosimetry. *Applied Radiation and Isotopes*, 52:1039-1050, 2000.
- [4] A Bartolotta, P Fattibene, S Onori, M Pantaloni, and E Petetti. Sources of uncertainty in therapy level Alanine dosimeters. *Applied Radiation and Isotopes*, 44(1/2):13-17, 1993.
- [5] M Anton. Development of a secondary standard for the absorbed dose to water based on the alanine EPR dosimetry system. *Appl. Radiat. Isot.*, 62:779-795, 2005.
- [6] A. Bakai, W. U. Laub, M. Alber, and F. Nüsslin. IMRT im Thoraxbereich: Überprüfung der Genauigkeit einer im Aldersonphantom berechneten Dosisverteilung mit Hilfe von Messungen und Monte-Carlo-Berechnungen. In *Jahrestagungsband der DGMP*, 1999.
- [7] I. Reng, J. Bohsung, J. Groll, U. Jahn, M. Stuschke, and V. Budach. Bestrahlungsplanung bei der intensitätsmodulierten Strahlentherapie. In *Jahrestagungsband der DGMP*, 1999.
- [8] B. Rhein, P. Häring, S. Götz, K.-H. Grosser, and R. Moschel. IMRT Verifikation am DKFZ Heidelberg - Ein Erfahrungsbericht nach über 100 IMRT Patienten. In *Jahrestagungsband der DGMP*, 2000.
- [9] Y. Morita, K Ohno, K Ohashi, and J Sohma. ESR Imaging Investigation on Depth Profiles of Radicals in Organic Solid Dosimetry. *Appl. Radiat. Isot.*, 1989.
- [10] G. R. Eaton, S. S. Eaton, and K. Ohno. *EPR Imaging and in vivo EPR*. CRC Press, 1991.
- [11] M Anton, H Weisen, M J Dutch, W von der Linden, F Buhlmann, R Chavan, B Marletaz, P Marmillod, and P Paris. X-ray tomography on the TCV tokamak. *Plasma Phys. Control. Fusion*, 1996.
- [12] W. H. Press, S. A. Teukolsky, W. T. Vetterling, and B. P. Flannery. *Numerical Recipes in Fortran, The Art of Scientific Computing*. Cambridge University Press, 2nd edition, 1992.
- [13] W. von der Linden. Maximum-entropy data analysis. *Appl. Phys. A*, 60:155, 1995.